Investigation on Ice Loads for Offshore Wind Turbine in Varying Ice Conditions

Proceedings of the Twenty-eighth (2018) International Ocean and Polar Engineering Conference **www.isope.org**
Sapporo, Japan, June 10-15, 2018

ISBN 978-1-880653-87-6; ISSN 1098-6189

Investigation on Ice Loads for Offshore Wind Turbine in Varying Ice Conditions

Wei Shi
State Key Laboratory of Coast and Offshore Engineering, Offshore Renewable Energy Research Center, Dalian University of Technology
Dalian, Liaoning, China

Xiang Tan
Nanyang Technological University
Singapore, Singapore

Li Zhou
School of Naval Architecture and Ocean Engineering, Jiangsu University of Science and Technology,
Zhenjiang, Jiangsu, China

Dezhi Ning
State Key Laboratory of Coast and Offshore Engineering, Offshore Renewable Energy Research Center, Dalian University of Technology
Dalian, Liaoning, China

Madjid Karimirad
Marine and Coastal Engineering, School of Natural and Built Environment, Queen's University Belfast,
Belfast, UK

ABSTRACT

The ice loading process has a clear stochastic nature due to variations in the ice conditions and in the ice-structure interaction processes of offshore wind turbine. In this paper, a numerical method was applied to simulate a monopile fixed-bottom and a spar-type floating wind turbine in either uniform or randomly varying ice conditions, where the thickness of the ice encountered by the spar were assumed to be constant or randomly generated. A theoretical distribution of the ice thickness based on the existing measurements reported in various literatures was formulated to investigate the response characteristics of the monopile wind turbine and spar wind turbine in such ice conditions. The effect of the coupling between the ice-induced and aerodynamic loads and responses for both operational and parked conditions of the rotor was studied. Moreover, the dynamic response of wind turbine in randomly varying ice was compared and verified with that of the wind turbine in constant ice.

KEY WORDS: offshore wind energy; ice loads; dynamic response; ice-structure interaction

INTRODUCTION

So far, more than 80% of the energy all over the world comes from fossil fuels. Excessive and improper use of fossil fuels has caused climate change and threatened human security and development. The Paris Agreement, which entered into force on 4 November, 2016, is a major step forward in the fight against global warming. Due to severe smog, forty Chinese cities reel under heavy air pollution. Air pollution becomes one of the key words in China in 2016 (PTI, 2016). Renewable energies play an important role for reducing greenhouse gas emissions, and thus in mitigating climate change. Offshore wind energy is recognized as one of the world's fastest growing renewable energy resources. By the end of 2015, totally 12,107 MW of offshore wind energy was installed around the world according to Global Wind Energy Council (GWEC) report (Fried, 2016). In Europe, 3230 turbines are now installed and grid-connected, making a cumulative total of 11,027 MW (Ho, 2016). However, governments outside of Europe have set ambitious targets for offshore wind and development is starting to take off in China, Japan, South Korea and the US. The 1.2 GW of capacity installed in Asia as of the end of 2015 was located China and mainly in Japan.

There is a large ambition for offshore wind energy in next ten years. According to new analysis from the International Renewable Energy Agency (IRENA) (Young, 2015), offshore wind power has the potential to grow from 12GW in 2015, to 100GW in 2030, driven by technology advancements and further cost declines. Researches of numerical modelling and the automatic control of offshore wind turbine

(OWT) have been carried out intensively (Shi, 2015a; Karimirad, 2015; Jiang, 2015). Approximately 20% of the European OWTs, which produce 10 GW in total, is to be installed in the Baltic Sea by 2020 based on a EWEA forecast (Arapogianni, 2013). Meanwhile, Bohai Bay in China and Great Lake in US also have significant potential for offshore wind energy. Two 300-MW offshore wind farms will be installed in Dalian Zhuanghe Offshore Wind Farm, which are located in the northern part of Bohai Bay in China, from 2017. Bottom-fixed wind turbines are mainly used due to shallow water depth in these areas (Shi, 2015b; Shi, 2013). Besides the aerodynamic and hydrodynamic, ice loads would also be an important load for OWTs in cold areas.

The challenges related to ice loads on OWTs are not well understood and have not been investigated in detail to date. Icing on OWT blades and drifting-level-ice-induced ice loads are main load sources that ice can affect wind turbines. Drifting ice could induce dynamic loads and may cause failure in the support structures of OWTs. This work only concentrates on the loads induced by level ice. Several studies have been performed on relevant feature for OWT. However, interaction between the level ice and OWT considering structure motion and velocity were not included.

The ice loading process has a clear stochastic characteristic due to variations in the ice conditions and ice breaking processes. A numerical method was introduced by Shi et al. (2016) to simulate the continuous ice breaking process between level ice and OWT. An inverted ice-breaking cone was attached to the monopile at the mean sea level (MSL) to reduce the ice loads on the structure. This numerical method used the dynamic ice bending model to consider the relative motion and velocities between structures and ice such that the monopile response influenced the interaction force between the cone and the ice. A series of icebreaking events were simulated and detailed contact information was observed based on the updated ice geometry. A dynamic link library (DLL) is used to feed the ice forces at each time step into the HAWC2 (Horizontal Axis Wind turbine simulation Code 2nd generation) based on the input position and velocity of the monopile using an iterative procedure.

In an earlier study, Shi et al (2016) investigated the ice loads on the monopile-type OWT under uniform ice conditions. In this paper, the ice model is extended to more complex ice conditions considering random ice thickness. And the numerical method is applied to simulate a spar-type FOWT (Floating Offshore Wind Turbine) interacting with drifting level ice under constant or randomly varying ice conditions. The responses are compared with the monopile wind turbine in similar conditions. The analysis shows the statistical variation of the loading process, which depends on the ice conditions, the contact and icebreaking pattern.

SIMULATION OF ICEBREAKING PROCESS

As previous mentioned, the numerical method that was introduced by Shi et al. (2016) is extended in this paper to simulate the ice-structure interaction for spar-type FOWT under more complex and variable ice conditions. In this part, the mode is briefly described again.

In this work, an icebreaking cone is deployed at the MSL to mitigate the ice loads by changing the failure modes from crushing to bending. To solve the equations of motion for the entire wind turbine system, the ice forces from the ice load model should be determined at each time step. The displacements of the structure at the MSL, which change the local slope angle of the structure, are taken into account by updating the waterline's geometry. The instantaneous waterline and the auxiliary waterline are discretized into nodes. Contact panels are constructed between two waterlines. The contact zones are assumed to be the overlaps between waterline and the ice edge. The contact area for each contact zone, A_{cr}, can be calculated based on the indentation depth, L_h, the inclination angle of the cone with the horizontal, φ, and ice thickness, h_i (Fig.1):

$$A_{cr} = \begin{cases} \frac{1}{2} L_h \frac{L_d}{\cos\varphi}, & L_d \tan\varphi \le h_i \\ \frac{1}{2}\left(L_h + L_h \frac{L_d - \frac{h_i}{\cos\varphi}}{L_d} \right) \frac{h}{\sin\varphi}, & L_d \tan\varphi > h_i \end{cases} \quad (1)$$

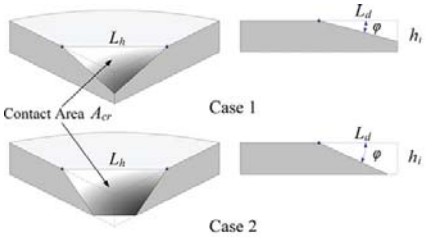

Fig. 1 Two cases of ice contact geometry (Su, 2010).

Before a bending failure occurs, we assume that the ice is only crushed on the contact surface. The local normal crushing force, F_{cr}, is calculated based on the contact area, A_{cr}, and the average crushing pressure, p_{av} (Fig.2):

$$F_{cr} = \begin{cases} -p_{av} A_{cr}, & v_2 \le 0 \\ 0, & v_2 > 0 \end{cases} \quad (2)$$

where the negative sign indicates that the force is always in the direction opposite to v_2.

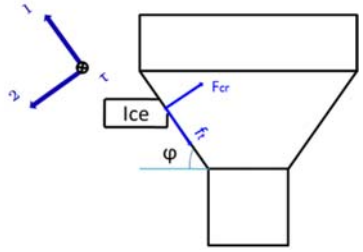

Fig. 2 Contact force and local coordinate system (Shi, 2016).

The average contact pressure, p_{av}, depends on the magnitude of the contact area, which is known as the pressure-area relation:

$$p_{av} = k A_{cr}^{n} \quad (3)$$

where k and n are empirical parameters, k is positive (1.23-1.51) and n is negative (-0.3 to -0.2).

The global ice force is determined by integrating local contact loads over the contact zones acting on the icebreaking cone simultaneously.

As the level ice impacts on the cone and continue to move passing the monopile, the contact area and the loads between the ice and cone increase. If the vertical component of the crushing and frictional forces exceeds the dynamic bending failure load P_f, given in Eq. (4), bending failure of the ice edge will occur and the broken ice pieces will be

cleared from the ice edge (Tan, 2014).

$$P_f = \left(1.65 + 2.47 v_2^{0.4}\right) \sigma_f h_i^2 \left(\frac{\theta_w}{\pi}\right)^2 \quad (4)$$

where, v_2 is the normal relative speed, σ_f is the bending strength the ice, $\left(\frac{\theta_w}{\pi}\right)^2$ is the geometry factor specifying the wedge size in the circumferential dimension.

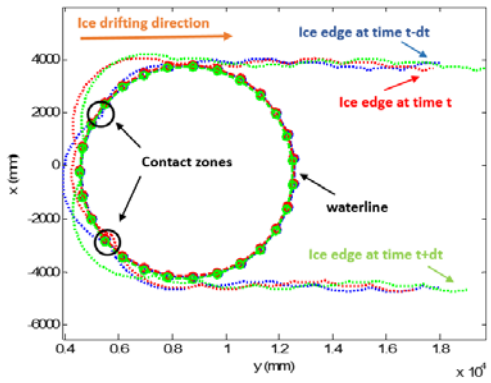

Fig. 3 Ice breaking pattern at different time.

Once the broken ice splits from the ice sheet, a new ice edge is constructed, and the next ice-structure interaction cycle begins (Fig.3). According to the assumptions and process, the icebreaking pattern and continuous icebreaking force can be calculated using step-by-step procedure.

SIMULATION RESULTS

Wind turbine system model

A 5 MW wind turbine model developed at NREL closely representing large mega-scale OWTs being manufactured today is used in our study. This model is a conventional variable speed, upwind, collective pitch horizontal axis wind turbine. The main properties of NREL 5 MW baseline wind turbine model are given in Table 1 (Jonkman, 2009).

Table 1. Main characteristics of the NREL 5 MW baseline OWT.

Parameter	Value
Rated power	5MW
Rotor Orientation	Upwind
Rotor, Hub Diameter	126 m, 3m
Hub height	90 m
Cut-In, Rated, Cut-Out Wind Speed	3 m/s, 11.4 m/s, 25 m/s
Cut-In, Rated Rotor Speed	6.9 rpm, 12.1 rpm
Overhang, Shaft tilt, Precone	5 m, 5 °, 2.5°
Rotor, Nacelle, Tower mass	110 t, 240 t, 347.46 t
Tower top, diameter, wall thickness	3.87 m, 0.019 m
Pile length, diameter	30 m, 6 m
Pile wall thickness, total weight	0.06 m, 187.9 t

The schematic layout of the offshore wind turbines is shown in Fig. 4.

The diameter of the monopile is 6 m. A water depth of 20 m is considered for monopile in this study. The pile was assumed rigidly connected to mudline. The ice-breaking cone used in this study is a 45º-inverted rigid cone with waterline width of 8 m. The cone is rigidly attached to the monopile at the MSL. For spar-type floating wind turbine, a catenary moored OC3-Hywind concept is considered in this article (Jonkman, 2010). The water depth of 320 m is assumed. Properties of the spar-type wind turbine are listed in Table 2.

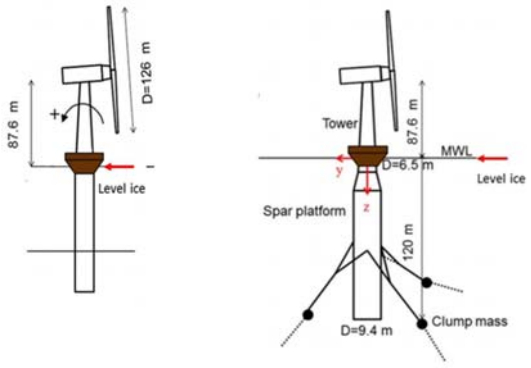

(a) (b)

Fig. 4 Schematic layout of the offshore wind turbine studied in this research (a) monopile (b) spar-type FOWT.

Table 2. Properties of the spar platform.

Parameter	Value
Water depth	320 m
Draft	120 m
Displacement	8016 m^3
Center of Buoyancy	-62 m
Diameter at MWL	6.5 m
Diameter at bottom	9.4 m
Mass	8216 ton
Center of gravity	-78.5 m
Mass moment of inertia, Ixx and Iyy	69.84E+6 ton*m^2
Mass moment of inertia, Izz	16.78E+4 ton*m^2
Fairlead elevation	-70 m

In this study, the coupled numerical simulations were carried out using HAWC2, which is developed at DTU. HAWC2 is an aeroelastic code intended for calculating wind turbine response in time domain. The code is based on a finite element formulation of the structural dynamics and an advanced blade element momentum (BEM) theory for the aerodynamics. The structural model is based on the multi-body formulation. The floating wind turbine is divided into several beams, each beam is a Timoshenko beam, and the beams are connected to each other by constraints. The dashpot, stiffness, ball joint and bearing are some of the modeling features in the HAWC2. In this article, HAWC2 is used to carry out the coupled aero-hydro-servo-elastic analyses for horizontal offshore wind turbine. The ice load is implemented as a user defined force through dynamic link library (DLL). At each iteration, the ice forces are calculated based on the current state variable of the icebreaking cone, current ice edge shape and cone-ice contact information. The calculated ice load vector is transferred to the node at the MSL in HAWC2 to solve the equation of motion of the wind

turbine system. The state variables are updated by the incremental values and the initial values at the beginning of the time step. According to the contact between the cone and ice edge, local contact speed, and material properties of the ice, a new ice edge is generated. In the analysis, the dynamic motion of the monopile is considered during the contact detection, which is neglected in the IEC and DNV standard.

Ice properties

The icebreaking cone used in this study is a 45-degree-inverted cone with waterline width of 8 m. It is assumed as a rigid body. Representative ice properties suggested by ISO standard for Baltic Sea are listed in Table 3 (ISO, 2010).

Table 3. Ice properties.

Parameter	Value
Density	880 kg/m^3
Crushing strength	2.3Mpa
Bending strength	580 kPa
Young's Modulus	5.4 GPa
Poisson ratio	0.33
Coefficient of friction	0.05
Ice sheet thickness	0.1 m~0.8 m
Ice drifting speed	0.1 m/s~0.5 m/s

In this work, the initial dataset for varying ice thickness was obtained from (Pfaffling, 2007) (Fig.5). They used the measurements from the "ARISE" expedition that took place in East Antarctica in 2003. The expedition involved drilling measurements of a level ice sheet including some ice ridges. By the extraction of the measurements these ridges were ignored and skipped, resulting the level ice field forming to the following shape (Fig.6).

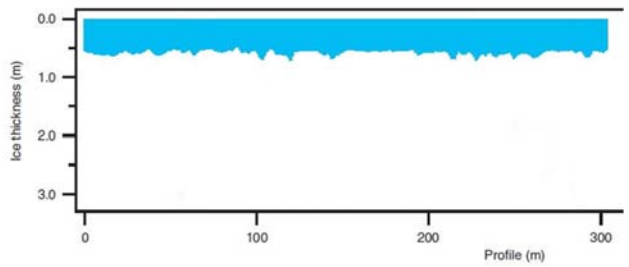

Fig. 5 Level ice field measurements (reproduced from Pfaffling, Haas and Reid 2007)

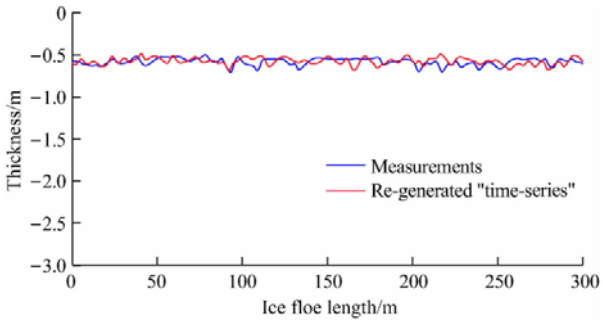

Fig. 6 Comparsion between the measured ice thickness and regnerated thickness.

Dynamic response in uniform ice conditions

The dynamic response of the monopile in uniform ice thickness was investigated assuming water depth of 20 m. The ice condition with 0.4 m thickness and 0.5 m/s drifting speed was considered. An external ice loads acting in the F-A direction at the MSL under different load cases were shown in Fig. 7. The ice-induced static load acting on the conical structure from IEC standard (IEC 61400-3, 2009) and the crushing force acting on the vertical monopile with same waterline diameter (Gravesen and Kärnä, 2009) (Dashed purple line in Fig.4) are also compared. Two different dynamic ice load models from the IEC standard are also used to determine the loads from the drifting ice on the conical structures (IEC 61400-3, 2009). The models from IEC and ISO standards are based on the 2D simultaneous failure assumption. Those models are based on prescribed, periodical ice load model. The 3D effect of ice–structure interaction and failure of local ice sheet are considered in our model, which induces a dynamic effect of ice loading. The numerical results from our model provide a stochastic behavior of the ice loading depending on the initial contact condition between the ice sheet and the monopile circumference at the MSL.

For a floating wind turbine, a NREL 5 MW turbine mounted on a spar buoy with water depth of 320 m is considered. In this section, the effect of level ice on the dynamic response of a monopile and a spar-type offshore wind turbine were investigated comparatively. The ice condition with 0.4 m thickness and 0.5 m/s drifting speed and wind speed of 18 m/s are assumed in different load cases. Meanwhile, both the operating and parked conditions are compared in this work. In Fig.8, the ice loads from different load cases are compared. The ice loads for spar-type FOWT are slightly smaller than the monopile due to large motion of floating wind turbine.

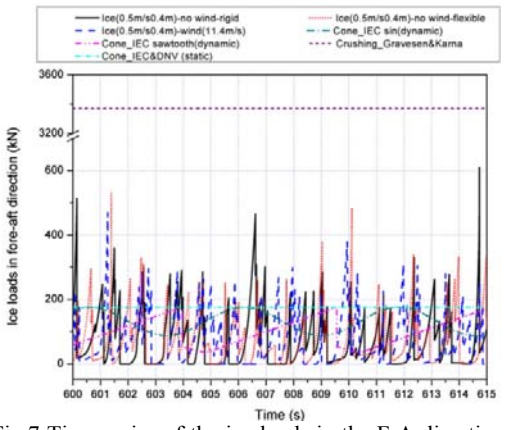

Fig.7 Time series of the ice loads in the F-A direction at the MSL (Shi et. al, 2016).

Fig. 9 gives the PSD of the ice loads in the F-A direction at the MSL for both monopile and spar wind turbine. For the monopile, all the load cases have same ice breaking frequencies because the relative motion of the structure is not significant. At loading frequency of 0.35 Hz, monopile under operating condition experiences smaller ice loads. For the spar, ice breaking frequencies shift between different load cases due to large relative motion. Non-simultaneous failure is dominant for spar-WT under operating.

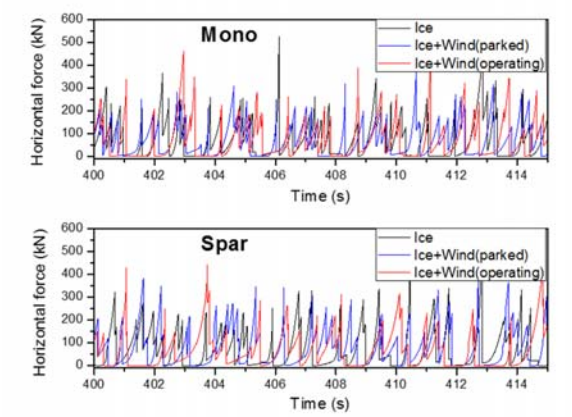

Fig. 8 Time series of the ice loads in the F-A direction at the MSL.

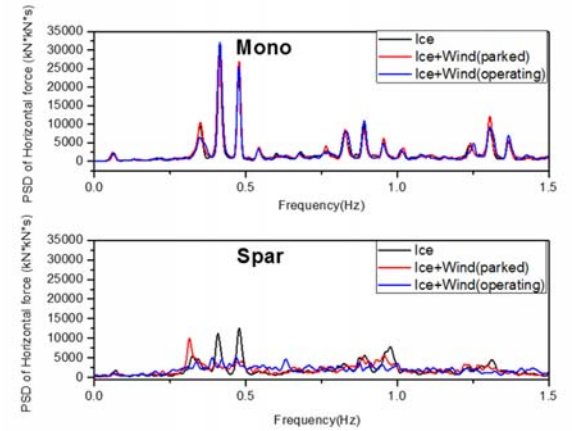

Fig.9 PSD of the ice loads in the F-A direction at the MSL.

The responses of the monopile-type and spar-type wind turbine were compared in Fig. 10. For the monopile, the second tower bending frequency (2.28 Hz) is clearly shown in the response for all the load cases. The response was reduced when the turbine is operating due to the aerodynamic damping. For the spar, largest energy content could be identified at platform roll/pitch natural frequencies (0.032Hz). Ice breaking frequency at around 0.5 Hz gives also arise of the response.

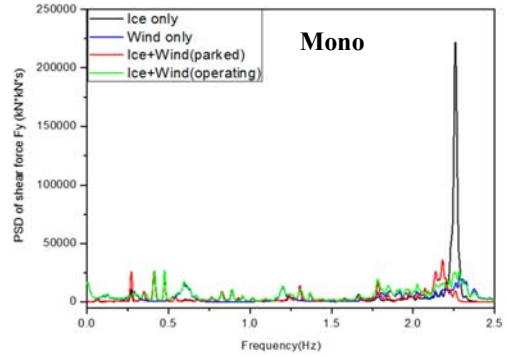

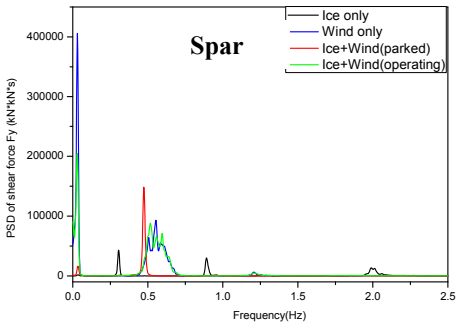

Fig.10 PSD of shear force in in the F-A direction at the MSL.

Dynamics response in varying ice conditions

In this section, the present numerical model was applied to simulate the monopile wind turbine interacting with drifting forward randomly varying ice conditions, where the thickness and strength properties of the ice encountered by the monopile were assumed to be constant or randomly generated. From Fig. 11, it shows that the ice loading process has a clear stochastic nature due to variations in the ice thickness and in the icebreaking processes of monopile. It can be observed that the ice loads show significant fluctuations and many load peaks are quite higher than the maximum value of the peaks coming from the constant thickness model.

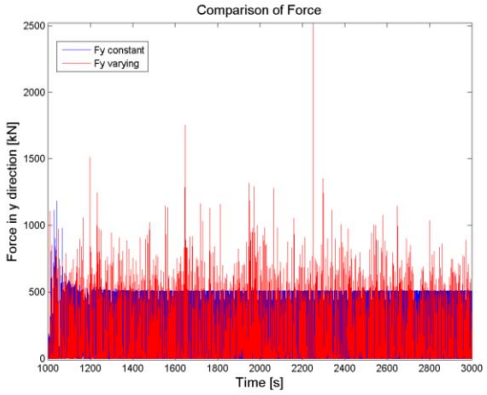

Fig.11 Time series of the ice loads in the F-A direction at the MSL for constant and varying ice thickness.

For the dynamic response of the wind turbine due to uniform or the varying ice thickness (Fig.12), there are more severe fluctuations of the response time series that induced by vary ice condition. For the varying thickness floe (Fig.13), there is a peak observed in 0.03 Hz, which is close to the roll/pitch/heave motion of the platform. However, most of the energy is concentrated at around 0.3 Hz.

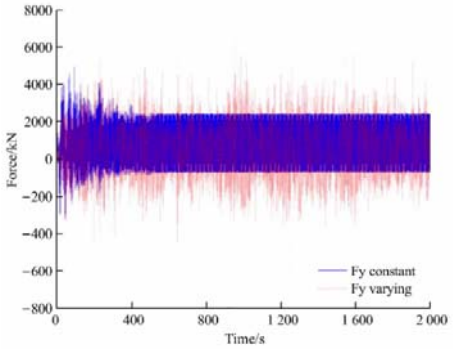

Fig.12 Time series of the shear force in the F-A direction at the MSL

for constant and varying ice thickness.

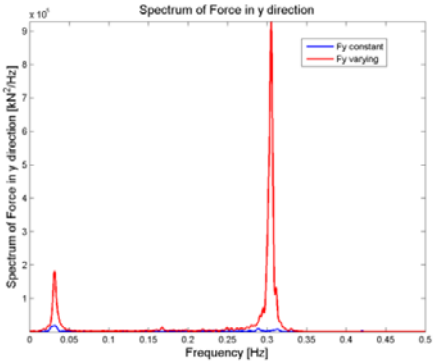

Fig.13 PSD of the shear force in the F-A direction at the MSL for constant and varying ice thickness.

CONCLUSIONS

A numerical ice-structure interaction model was implemented to aero-hydro-servo-elastic tool, HAWC2, to investigate the ice load effect on monopile and spar offshore wind turbines. The dynamic response of the monopile and spar wind turbine due to ice-induced loads were compared comprehensively. And the ice load were also compared with the models from IEC and ISO standards. The present numerical model could reveal more the ice-structure interaction between level ice and wind turbine. Although the aerodynamic loads from wind flow is the dominant in the design, the ice loads from level ice has very important influence on the dynamic response of the wind turbine.

It is observed that the varying ice thickness field will increase the dynamic effect of the ice loads, thus introduces a more dynamic effect on the structure. This will be further investigated to study the effect of stochastic ice loads on the dynamic response of offshore wind turbine.

ACKNOWLEDGEMENTS

The authors would like to gratefully acknowledge financial support from the National Natural Science Foundation of China (Grant No. 51709039, 51379032 and 51490672). This work is partially supported by the international collaboration and exchange program from the NSFC-RCUK/EPSRC with grant No. 51761135011.

REFERENCES

Arapogianni, A, Genach, AB (2013). "Deep water—the next step for offshore wind energy," European Wind Energy Association (EWEA).

Fried, L, Qiao, L, Sawyer, S and Shukla S (2016). *Global Wind Report. Annual market update 2015*.

Gravesen, H, Kärnä, T (2009). "Ice loads for offshore wind turbines in Southern Baltic Sea," *Proc. 20th International Conference on Port and Ocean Engineering under Arctic Conditions (POCA'09)*, Luleå, Sweden, June 9–12.

Ho, A, Mbistova, A, and Corbetta, G (2016). *The European offshore wind industry-key trends and statistics 2015*. Report. Brussels: European Wind Energy Association.

IEC 61400-3 (2009). Wind turbines, Part 3: Design requirements for offshore wind turbines. IEC.

ISO 19906, 2010. *Petroleum and Natural Gas Industries-Arctic Offshore structures*. International organization for standardization, ISO 19906, Geneva, Switzerland.

Jiang, ZY, Xing, YH, Guo, Y, Moan, T, and Gao, Z (2015). "Long‐term contact fatigue analysis of a planetary bearing in a land‐based wind turbine drivetrain," *Wind Energy*, 18(4), 591-611.

Jonkman, J, Butterfield, S, Musial, W, Scott, G (2009). *Definition of a 5-MW reference wind turbine for offshore system development*. Golden, CO, National Renewable Energy Laboratory. NREL Report TP-500-38060.

Jonkman J, Larsen T, Hansen A, et al. Offshore Code Comparison Collaboration within IEA Wind Task 23: Phase IV Results Regarding Floating Wind Turbine Modeling, P*roceedings of the European Wind Energy Conference (EWEC)*, National Renewable Energy Laboratory, Warsaw, Poland; April 2010.

Karimirad, M, and Michailides, C (2015). "V-shaped semisubmersible offshore wind turbine: An alternative concept for offshore wind technology," *Renewable Energy*, 83, 126-143.

Pfaffling, A, Christian H, and James ER (2007). "Direct helicopter EM - Sea-ice thickness inversion." *Geophysics*, 72.

PTI, http://timesofindia.indiatimes.com/world/china/40-chinese-cities-reel -under-heavy-pollution-for-3rd-day/articleshow/56050510.cms.[Online] [Accessed 18 December, 2016]

Shi, W, Park, HC, Chung, CW, Shin, HK, Kim, SH, Lee, SS, and Kim, CW (2015a). "Soil-structure interaction on the response of jacket-type offshore wind turbine," *International Journal of Precision Engineering and Manufacturing-Green Technology*, 2(2), 139-148.

Shi, W, Han, J, Kim, C, Lee, D, Shin, H, and Park, H (2015b). "Feasibility study of offshore wind turbine substructures for southwest offshore wind farm project in Korea," *Renewable Energy*, 74, 406-413.

Shi, W, Park, HC, Han, JH, Na, SK, Kim, CW (2013). A study on the effect of different modeling parameters on the dynamic response of a jacket-type offshore wind turbine in the Korean Southwest Sea," *Renewable Energy*, 58, 50–59.

Shi, W, Tan, X, Gao, Z, and Moan, T (2016). "Numerical study of ice-induced loads and responses of a monopile-type offshore wind turbine in parked and operating conditions," *Cold Regions Science and Technology*, 123, 121-139.

Su, B, Riska, K, Moan, T (2010). "A numerical method for the prediction of ship performance in level ice," *Cold Regions Science and Technology*, 60, 177–188.

Tan, X, Riska, K, Moan, T (2014). "Effect of dynamic bending of level ice on ship's continuous-mode icebreaking," *Cold Regions Science and Technology*, 106–107, 82–95

Young, E (2015). *Offshore wind in Europe: walking the tightrope to success*. Paris: Ernst & Young.

\Conf-std\Template-Word-MS-2018 (0928-2017)